Lab Invest 106 (2026) 106156

LABORATORY INVESTIGATION

journal homepage: https://laboratoryinvestigation.org/

USCAP Advancing Pathology Together

Research Article

Development of a Novel Immunohistochemistry Assay to Characterize Extradomain-B of Fibronectin (EDB+FN) Protein Expression in Solid Tumors

Sara L. Lewandowski[a,*], Chuan Shen[a], Liyang Diao[a], Alyssa M. Quigley[a], Tracy Brennan[b], Timothy Cloherty[b], Tenzin Dolker[b], Richard Siderits[b], Jan Pinkas[a], Marsha L. Crochiere[a]

[a] *Pyxis Oncology, Department of Translational Medicine and Research, Boston, Massachusetts;* [b] *Discovery Life Sciences, Newtown, Pennsylvania*

ARTICLE INFO

Article history:
Received 23 December 2025
Revised 21 July 2026
Accepted 23 July 2026
Available online 30 July 2026

Keywords:
cancer
digital pathology
extradomain-B of fibronectin
immunohistochemistry
micvotabart pelidotin
tumor stroma

ABSTRACT

Purpose: Tumor stroma, the cellular and noncellular support system surrounding cancer cells, is a promising source of novel therapeutic targets. Extradomain-B of fibronectin (EDB+FN), a tumor-specific antigen expressed in the extracellular matrix of tumor stroma and minimally in healthy tissues, is the target of the first-in-concept antibody-drug conjugate micvotabart pelidotin, which is currently in clinical trials (NCT05720117 and NCT06795412) for the treatment of solid tumors. A specific and reproducible immunohistochemistry (IHC) assay and scoring approach are needed to detect EDB+FN protein expression for indication selection, preclinical research, and potential future evaluation of correlations between target expression and therapeutic efficacy.
Materials and Methods: An EDB+FN IHC assay was developed to detect EDB+FN protein in human solid tumors. A novel scoring system was developed, adapting the H-score methodology to evaluate the intensity and localization of EDB+FN extracellularly in tumor stroma and cellularly in cancer cells in 10 solid tumor types. Moreover, a custom, artificial intelligence–powered digital pathology algorithm was developed to streamline scoring of EDB+FN protein expression for research and future analysis of spatial distribution.
Results: The developed IHC assay reproducibly detected EDB+FN in the tumor stroma across formalin-fixed paraffin-embedded samples from 10 tumor types and minimally in normal tissue. Percent stroma was not predictive of EDB+FN expression within a tumor, suggesting heterogeneous EDB+FN protein expression in tumor stroma. The modified H-scoring approach reproducibly quantified EDB+FN expression extracellularly in tumor stroma by pathologist evaluation, and a digital algorithm built with open-source tools demonstrated proof-of-concept for digital quantification of EDB+FN protein expression.
Conclusions: This study demonstrates technical characterization of a research-use IHC assay for detection of EDB+FN in formalin-fixed paraffin-embedded tumor sections, reveals broad expression of EDB+FN across cancer types, and establishes a novel approach for scoring expression of a non–cell-associated protein in the tumor extracellular matrix, both by pathologists and using digital pathology.

* Corresponding author.
E-mail address: slewandowski@pyxisoncology.com (S.L. Lewandowski).

https://doi.org/10.1016/j.labinv.2026.106156

Introduction

The development of therapies targeting cancer cell membrane antigens has improved the life expectancy of patients with cancer.[1] However, cancer remains the second most common cause of death in the United States, and new treatment options are needed to reduce mortality rates. With the more recent success of immune checkpoint and vascular endothelial growth factor inhibitors in solid tumors, the tumor microenvironment (TME) is of high interest for the development of novel targeted cancer treatments.[2-10]

The TME is a complex and dynamic interplay of cancer cells with immune cells, tumor stromal cells, blood vessels, and extracellular matrix (ECM) components and is capable of influencing tumor growth, metastasis, and invasion.[11,12] Within the TME, the tumor stroma not only serves as a structural and facilitating scaffold for tumor cell migration but also enables the tumor to withstand harsh conditions such as hypoxia, high metabolic demand, and chemotherapeutic attack and modulates immune infiltration and immune cell activation, contributing to treatment resistance.[11-13] Indeed, a high relative amount of stroma throughout the tumor tissue, termed the tumor-stroma ratio, has been correlated with poor clinical prognosis in several solid tumor cancer types.[14] Despite the importance of the stroma in cancer progression and prognosis, few therapeutics have been developed to specifically target stromal cells and ECM proteins.[15]

The ECM of the tumor stroma consists of multiple components, including collagen[16,17] and fibronectin (FN)[13,18] isoforms that are differentially expressed in tumors compared with healthy tissues.[16,17] Quantification of these differences can offer prognostic value to patients and physicians.[17,19,20] Of particular interest is extradomain-B of fibronectin (EDB+FN), which is a secreted, non-membrane-bound, oncofetal splice variant of FN that is abundant in the ECM of tumors and largely absent in healthy adult tissues.[21,22] EDB+FN is secreted from a variety of cell types in tumors, including endothelial cells of newly formed blood vessels, stromal cells, including myofibroblasts, and cancer cells.[21,23-25] Moreover, the expression of EDB+FN is associated with tumor growth, angiogenesis, and metastasis,[22,26] highlighting the potential as a therapeutic target and as a biomarker for diagnosis and prognosis for a number of tumor types.[19-21,27-29] Currently, EDB+FN is being evaluated as a clinical target with the novel antibody-drug conjugate micvotabart pelidotin (MICVO, previously known as PYX-201)[30] as a monotherapy as well as in combination with pembrolizumab for the treatment of solid tumors in phase 1/2 clinical trials (NCT05720117 and NCT06795412). Having an assay to evaluate target expression in human tumor samples and animal models would be beneficial for indication selection, mechanism of action studies, and analyzing correlations between target expression and drug efficacy.

To date, several assays have been developed to evaluate EDB+FN expression using both imaging and molecular techniques depending on cancer type and location. Quantitative PCR, gene expression analysis, such as using microarray, immunoaffinity liquid chromatography–mass spectrometry, and enzyme-linked immunosorbent assays are efficient to detect low levels of *EDB+FN* RNA or EDB+FN protein expression, but lack spatial resolution.[20,22,27,31] Imaging studies such as in vivo positron emission tomography and single-photon emission computed tomography can detect EDB+FN in vivo using the highly specific L19 monoclonal antibody targeting the EDB domain of FN, the same antibody clone used in EDB+FN-targeting therapeutics, including MICVO.[30,32-35] However, the most utilized assay for protein detection in solid tumor biopsies is immunohistochemistry (IHC).[36] There are several effective options available for assessing EDB+FN protein expression in frozen tissue samples, including 3,3′-diaminobenzidine (DAB) and fluorescence staining with several antibody clones[30,37] and direct fluorescent labeling using L19-fluorescein isothiocyanate.[38] Multiple antibody clones have even been compared head-to-head for detection in frozen tissue sections.[39] However, EDB+FN epitope instability has been reported in frozen tissue sections, limiting utility for stored samples.[39,40] Although there are several methods for EDB+FN detection in formalin-fixed paraffin-embedded (FFPE) tissue samples using an alkaline phosphatase/anti–alkaline phosphatase method combined with anti-EDB antibody clones L19 or G4, there is no technically validated assay and scoring method to effectively quantify EDB+FN protein expression in FFPE tumor samples.[21,34] Considering the wide use of FFPE tissues, both clinically and nonclinically, it would be advantageous to have a standardized and validated method for detection of EDB+FN in paraffin-embedded samples.[36] Likewise, a robust scoring algorithm is essential to capture and quantify both the intensity and distribution of EDB+FN expression within these tissue samples. Although global, qualitative scoring metrics have been used to characterize EDB+FN expression, a validated assay with more quantitative metrics has not been established.

Several numeric scoring approaches are utilized for cellular targets, including histochemical (H)–score, which can be applied to tumor samples to reliably examine protein expression within specific cell types of interest.[41] This method has been important in determining relationships between other proteins and tumor characteristics and is used in diagnosis, prognosis, predicting therapy response, stratifying patients, and in treatment decisions.[42,43] Noncellular targets, such as EDB+FN, do not have similar established scoring methods to quantify intensity and distribution of expression. Adaptation of cell-based scoring algorithms for noncellular targets could fill this gap, allowing for reproducible scoring for preclinical investigation of noncellular targets and future clinical applications.

Here, a research-use IHC assay was developed to assess the expression of the non–cell-associated protein EDB+FN in the stroma of solid tumors and normal human tissues. Based on the heterogeneous expression of EDB+FN protein,[27] the novel IHC assay was calibrated to detect a broad range of EDB+FN expression using a modified H-score to assess both intensity and distribution of EDB+FN expression in cancer cells and extracellularly in tumor stroma. An accompanying digital pathology algorithm was developed utilizing existing open-source tools, further demonstrating assessable adaptations of cell-focused pathology approaches for extracellular targets. This research-use IHC assay and scoring approach has potential utility in informing indication selection and mechanism of action studies, as well as the potential for future development into a laboratory-developed test to inform patient selection for EDB+FN-targeting therapeutics, including the clinical candidate MICVO.

Materials and Methods

Evaluation of Extradomain-B of Fibronectin Gene Expression From Public Database

To determine nominal *EDB+FN* RNA expression levels in normal and tumor tissues, RNA-Seq expression data were

procured from the QIAGEN OncoLand database (release B38, data versions CCLE_B38_20190215_v7, GTEx_B38_20190215_v4, and TCGA_B38_20190215_v8). The QIAGEN OncoLand database is a curated database of expression and other genomic data, including data from The Cancer Genome Atlas (TCGA), the Genotype Tissue Expression (GTEx) project, and the Cancer Cell Line Encyclopedia (CCLE). The data set included 11,291 tumor and tumor-adjacent normal samples from TCGA, 9052 normal tissue samples from GTEx, and 932 cell lines from CCLE. The data consisted of 33 solid and liquid cancer types from TCGA and 89 cancer types from CCLE, representing 54 tissues from 23 broad tissue categories. Expression in tumor and normal samples was compared based on tissue and broad tissue categories, such as by organ system, for example, the urinary system, or tissue type, for example, glandular tissue. However, it is important to note that not all tumor samples have matched normal samples. Of the 102 cancer types evaluated, there were ultimately 43 cancer types for which there were sufficient tumor and/or normal samples for which a *t* test could be performed (minimum N = 3), when matched normal tissue was used for comparison. When using broader tissue categories as normal background, 71 cancer types were evaluable.

EDB+FN RNA expression was evaluated by first mapping the *EDB+FN* sequence to the human genome (hg38) to determine sequence overlap using IGV BLAT (v2.11.9).[44,45] Three transcripts (Ensembl release 94) were found to coincide with the EDB region, and the summed expression across these 3 transcripts was used to determine the expression of *EDB+FN*. Boxplots were generated using the R (R Core Team) package ggplot2,[46] grouping tumor samples by Tissue and Tissue Category values, respectively, to compare the distribution of expression values of the target *EDB+FN* against normal tissue expression. RNA expression values were log-transformed prior to plotting by taking log (fragments per kilobase of transcript per million mapped reads (*FPKM*) + 0.1). These data were subsequently used to select a subset of tumor tissues to be evaluated in the IHC assay.

Immunohistochemistry Assay Development

Two primary antibodies were evaluated for IHC in FFPE human tissues: anti-EDB+FN Clone L19[35] (monoclonal rabbit immunoglobulin G [IgG], Pyxis Oncology) and anti-EDB+FN Clone G4[35] (monoclonal rabbit IgG, Pyxis Oncology), subsequently referred to as L19 and G4, respectively. Human tumor and normal tissues were sourced from the Discovery Life Sciences (Goleta, CA; Newtown, PA) tissue bank and the Maine Medical Center Biobank. The TechMate IHC platform (Dako) and Leica BOND III Platform (Leica Biosystems) were used in the initial assay development for the visualization of the IHC signal. Once initial conditions were identified, further testing and development were performed with the Leica BOND III Platform. Several concentrations of the antibodies were tested to determine the optimal dilution range for the IHC assay. L19 was evaluated at concentrations ranging from 0.5 to 6 μg/mL, and G4 was evaluated at concentrations ranging from 1 to 8 μg/mL. The optimal staining range was determined by manual review of IHC signals across tumor samples from multiple cancer types, selecting antibody concentrations that balanced detection of weak signal over background and discrimination of strong signals below the level of signal saturation. Optimized staining conditions of each antibody were then tested on human tissues, and staining patterns were compared between antibody candidates.

Immunohistochemistry Assay Scoring Criteria

To quantify the expression of EDB+FN in the ECM, a modified H-score approach was developed. Adapting the traditional H-score approach of weighted percentages of cells at differing intensity levels, this modified H-score approach evaluated weighted percentages by area at differing intensity levels, accommodating the noncellular expression profile of EDB+FN in the ECM. Four sets of H-scores were generated by a board-certified pathologist (T.C. or R.S.) for tumor samples, one evaluating cancer cell membrane and tumor stroma tissue collectively ("total"), one evaluating only tumor stroma ("stroma"), and 2 evaluating only cancer cells, either cancer cell membrane or cancer cell cytoplasm. Tumor stroma was defined as stroma within the tumor field, excluding normal stroma outside the tumor field. IHC scoring in normal tissue was performed for total tissue and separately for staining in normal stroma, as well as the plasma membrane and cytoplasm in nonstromal cell types. Areas of ischemic changes, thermal artifact, and necrosis were excluded from scoring in all samples. The percentage, by area, of EDB+FN protein expression at differential intensity levels were determined on a 4-point numeric scale (0, 1+, 2+, 3+) within each of the scoring regions, with the values defined as: 0 = null, negative or nonspecific staining; 1+ = low or weak staining; 2+ = medium or moderate staining; and 3+ = high or strong staining. The H-score for the IHC staining was determined by summing the percentage, by area, of an expression intensity multiplied by its corresponding differential intensity on the 4-point semi-quantitative scale (0, 1+, 2+, 3+), with scores ranging from 0 to 300. The H-score was calculated as follows: H-score = [(% at <1) × 0] + [(% at 1+) × 1] + [(% at 2+) × 2] + [(% at 3+) × 3]. Tumor H-score sums were calculated from human tumor samples as combined cancer cell plasma membrane and cytoplasmic staining H-scores (sum of individual H-scores for each subcellular localization) and had a possible range from 0 to 600 (from combining 2 values with ranges from 0 to 300).

Assay Characterization

Technical characterization of the developed assay conditions for research use, utilizing the L19 antibody, was performed to assess specificity, precision, reproducibility, and epitope stability.

To evaluate specificity, IHC staining was performed on FFPE cell pellets prepared from cell lines expressing varying levels of endogenous *EDB+FN* RNA expression. The cell lines, in order of increasing *EDB+FN* RNA expression, were HEL92.1.7, H358, T98G, CAKI-1, SK-MEL3, SKNSH, and CAKI-2, all from ATCC. A rabbit IgG isotype control antibody (DA1E, Cell Signaling) was used to evaluate the background signal. A species-matched positive control tissue and stain were used to confirm the function of the detection reagents.

The binding specificity of L19 was further characterized using biolayer interferometry analysis on an Octet RED96e instrument (Sartorius) at 25 °C. This was used to verify the specificity of the L19 clone, but does not replace IHC assay–specific specificity testing. Octet NTA Biosensors (Sartorius, Cat#18-5101) were soaked in assay buffer (1× phosphate-buffered saline containing 0.1% bovine serum albumin and 0.02% Tween 20, pH 7.2) for at least 10 minutes. Fifty nanomolar native or heat-denatured (100 °C, 15 minutes), His-tagged, recombinant FN variants hFN_7EDB89 (Wuxi Biologics), hFN_11EDA12 (made in-house), and hFN_S607-P1265 (SinoBiological, Cat#10314-H08H) were

separately loaded onto the NTA biosensors for 2 minutes. The NTA biosensors were then dipped into assay buffer for 2 minutes to reach the baseline. For the association step, the NTA biosensors were submerged into wells containing 25, 12.5, 6.25, 3.13, 1.56, 0.78, 0.39, and 0 nM of purified L19 antibody, human FN antibody (R&D Systems, Cat# MAB19182), and FN (IST-9) monoclonal antibody (Santa Cruz, Cat# sc-59826) in assay buffer for 5 minutes, respectively. Then, in the dissociation step, the NTA biosensors were dipped into assay buffer for 10 minutes to acquire data. The data were analyzed using Octet Data Analysis software HT 12.0.2.59. The sensorgrams were subtracted from the reference and globally fitted into a 1:1 binding model for data analysis.

To evaluate the reproducibility of the IHC staining, a pilot-scale evaluation was conducted in which serial sections from 9 tumor samples, representing 6 cancer types, were stained in triplicate across 2 independent staining runs, each run performed by a different operator. All stained sections were scored by the same board-certified pathologist (T.C.) following the modified H-score criteria. Intraoperator and interoperator reproducibility were assessed using the coefficient of variation (%CV), with acceptance criteria set as below 20% CV, and Bland–Altman analysis, with bias calculated as the mean difference between operators and 95% limits of agreement (LoA) defined as the mean difference ± 1.96 SDs. Analyses were performed, and plots were generated using the dplyr,[47] tidyr,[48] BlandAltmanLeh,[49] and ggplot2[46] packages in R (R Core Team).

To evaluate epitope stability in cut FFPE slides over time, a pilot series of sequential sections was cut from each of 3 tumor blocks, mounted to slides, dried, and stored at room temperature for the following lengths of time: 0 weeks, 4 weeks, 8 weeks, 12 weeks, 24 weeks, 36 weeks, and 52 weeks. The selected tumor blocks represented 3 cancer types—pancreatic cancer, thyroid cancer, and head and neck cancer—and had previously shown a range of stromal EDB+FN expression. After the set storage durations, one stored slide from each tumor block was tested using the developed IHC assay and scored by a board-certified pathologist (R.S.). Scores for each tumor sample were compared across storage time points using the %CV to determine epitope stability.

Immunohistochemistry Screening

Based on the data from the RNA-Seq analysis, 10 cancer types were selected for screening: thyroid carcinoma, head and neck squamous cell carcinoma (HNSCC), triple-negative breast cancer (TNBC), hormone receptor–positive breast cancer, hepatocellular carcinoma, soft tissue sarcoma, pancreatic cancer, non–small cell lung cancer (NSCLC), ovarian cancer, and renal cell carcinoma. Human whole tissue FFPE samples and multitissue FFPE blocks were sourced from Discovery Life Sciences (Goleta, CA; Newtown, PA) or from the Maine Medical Center Biobank (Portland, ME). Pancreatic cancer samples were primarily ductal adenocarcinoma; NSCLC samples were an even split of adenocarcinoma and squamous cell carcinoma; ovarian cancer samples included a mix of endometrioid carcinoma, mucinous carcinoma, serous papillary carcinoma, and clear cell adenocarcinoma; and sarcoma samples included a variety of subtypes. A total of 210 cancer tissue samples, consisting of approximately 20 samples per cancer type, were evaluated for EDB+FN expression by IHC. A human normal tissue microarray containing 89 intact cores representing 33 tissue types, with tissues collected and documented under conditions that meet US Food and Drug Administration–related requirements for human tissue sourcing, consent, and handling (Pantomics MNO961) was evaluated in parallel. A previously evaluated multitissue block containing human tissues of various cancer types and one normal tissue served as expression controls for EDB+FN. A rabbit IgG isotype control antibody (DA1E, Cell Signaling) was used to evaluate nonspecific staining. A species-matched positive stain (CD3, Dako/Agilent) and tissue (tonsil) were used as a run control to confirm the function of the detection reagents.

Tissue blocks were sectioned at 4 to 5 μm, mounted on SuperFrost Plus charged glass slides (Fisher), and allowed to dry overnight. Each sample was serially sectioned for IHC and staining with hematoxylin and eosin to assist in tumor morphology assessment and scoring. Automated processing was performed on a Leica BOND III IHC staining platform. Tissue sections were briefly heated at 60 °C for 30 minutes and dewaxed with Leica BOND Dewax solution. Sections were then processed for epitope retrieval using Leica BOND high pH epitope retrieval solution (Tris EDTA, pH 9). Sections were heat-treated at 100 °C for 20 minutes, followed by a Proteinase K digestion at 37 °C, and blocking with Leica Refine peroxidase blocking solution for 5 minutes. L19 was applied at 1.5 μg/mL for 1 hour at room temperature. This concentration was selected to provide a wide staining range to fully capture weak, moderate, and strong expression. Tissue sections were then washed (BOND wash buffer) and incubated with anti-mouse IgG linker (Leica) for 8 minutes, followed by a wash and incubation with horseradish peroxidase polymer for 8 minutes and washed again. The chromogen DAB was applied for 10 minutes, washed, and counterstained with hematoxylin for 5 minutes. Slides were then dehydrated in an alcohol series and cleared with xylene before coverslipping with Cytoseal (Thermo Scientific). Sections were scored by a board-certified pathologist from Discovery Life Sciences (T.C.). To determine the amount of tumor stroma, hematoxylin and eosin–stained slides were evaluated by a board-certified pathologist (T.C.). EDB+FN staining in the tumor and stromal compartments was scored using the modified H-scoring approach and imaged at ×20 using an Aperio AT2 slide scanner with Aperio Console version 10.2.0.7.5.

Development of Digital Pathology Algorithm

A digital pathology algorithm was developed for the streamlined assessment of EDB+FN protein expression in nonclinical samples, similar to those evaluated here. Briefly, using Qupath software[50] (version 0.3.2), tissue was identified using the standard tissue identifier in Qupath and manually reviewed to exclude artifacts. The tissue area was segmented into “cells” using the default cell classifier function in Qupath, which segmented both cancer cells and cellular and noncellular regions of stroma into “cells.” A tumor/stroma classifier was trained with multiple examples of tumor and stroma morphology, both EDB+FN expressing and EDB+FN negative, from EDB+FN IHC-stained sections across a range of cancer types. This classifier was applied to categorize individual “cells” within each slide scan as either cancer or stroma. Combined areas of each category (cancer and stroma) were used to compute percent stroma using R. To quantify EDB+FN protein expression, IHC staining intensity thresholds were developed to correspond to the 4-point numeric scale (0, 1+, 2+, and 3+) used in pathologist H-scoring. Data from each “cell,” including classification as cancer, stroma, and intensity threshold, were exported from Qupath and processed in R. To identify the appropriate intensity thresholds, a “training set” of 40 samples was randomly selected from the 210 tumor samples previously scored by a pathologist (T.C.) and was evaluated using Qupath cell thresholders and a grid search algorithm.

Briefly, a series of 37 incrementally increasing intensity thresholds was applied to each slide scan, and the percentage of tumor or stroma cells at each threshold was determined. The range of selected thresholds spanned from a minimum DAB intensity value that captured both true staining and all background signal, to a maximum value above which no staining was detected. A grid search was performed using R to evaluate each combination of 4 intensity ranges, computing the median deviance from pathologist scores across all 40 samples for each combination of thresholds. The best-fitting set of thresholds was identified based on the lowest median deviance from pathologist scores. To validate the thresholds, an independent "validation set" of 40 samples was randomly selected from the remaining set of pathologist-scored samples and evaluated by applying the trained tumor/stroma classifier, followed by the identified set of cell intensity thresholds. The combined area of each sample at each intensity interval was determined, and digital H-scores were calculated as follows using R: digital H-score = [(% at <threshold 1) × 0] + [(% at threshold 1+) × 1] + [(% at threshold 2+) × 2] + [(% at threshold 3+) × 3]. Agreement between pathologist scores and digital scores was evaluated for both the training set and validation set using Bland–Altman analysis, with bias calculated as the mean difference between pathologist and digital scores and 95% LoA defined as the mean difference + 1.96 SD. Analyses were performed, and plots were generated using the dplyr,[47] tidyr,[48] BlandAltmanLeh,[49] and ggplot2[46] packages in R.

Reproducibility of the developed digital algorithm was evaluated utilizing scans of the slides used to test the reproducibility of the IHC assay, described above. Triplicate serial sections of each of the 9 tumor samples, stained in each of 2 staining runs by different technicians, were scored using the digital scoring algorithm. Reproducibility was assessed using the %CV, considering both intrarun replicates and interrun replicates separately and combined, and Bland–Altman analysis with bias calculated as the mean difference between operators and 95% LoA defined as the mean difference ± 1.96 SD. Analyses were performed, and plots were generated using the dplyr,[47] tidyr,[48] BlandAltmanLeh,[49] and ggplot2[46] packages in R.

Results

Extradomain-B of Fibronectin Gene Expression in Tumor and Normal Tissue

To understand the expression profile of *EDB+FN* across solid tumors, a total of 10,550 primary tumor and 9793 normal human tissue samples from the QIAGEN OncoLand database were assessed for *EDB+FN* RNA expression. Over 2 dozen cancer types showed significantly elevated *EDB+FN* RNA expression compared with their relevant normal tissues. Among the cancer types with the greatest difference in gene expression between tumor and normal tissue were thyroid cancer, several kidney cancers, pancreatic cancer, melanoma, breast cancer, glioblastoma, and liver cancer (Fig. 1A, $P < .05$ for all). When stratified based on tissue categories, rather than individual tissue types, additional cancer types showed differential *EDB+FN* RNA expression, including several gliomas (based on cell line data) and sarcomas (Fig. 1B). The highly differential expression of *EDB+FN* RNA across multiple cancer types, coupled with relatively low overall normal tissue expression, positioned EDB+FN as a promising therapeutic target. Several tumor types with high differential *EDB+FN* gene expression and others of clinical interest were selected to evaluate EDB+FN protein expression.

Immunohistochemistry Assay Optimization

To develop a specific and reproducible method for evaluating EDB+FN protein expression, a research-use IHC assay was developed, and technical characterization was performed on several solid tumor types with differential *EDB+FN* expression, as identified by gene expression analysis, as well as cancer types of clinical interest. Initial IHC assay development optimized conditions for 2 primary antibody clones, L19 and G4, on both the TechMate and the Leica BOND III as described in Supplementary Table S1. Staining range optimization evaluated L19 and G4 concentrations that ranged from 1 to 6 μg/mL and 1 to 8 μg/mL, respectively. The optimal antibody concentrations for IHC staining that showed a wide range of staining intensities in tumor samples with minimal background were the following: 2.5 μg/mL (without Proteinase K) or 5.5 μg/mL (with Proteinase K) for G4 and 1.5 μg/mL for L19 (Supplementary Fig. S1A). While the L19 assay conditions were developed using Proteinase K, staining is comparable with and without Proteinase K across 3 tested samples reflecting different cancer types and levels of EDB+FN expression, suggesting that this step may be optional (Supplementary Fig. S1B). Staining with G4 showed diffuse expression across both tumor parenchyma and tumor stromal compartments, inconsistent with the known biology of EDB+FN as a component of the tumor ECM. In contrast, staining with L19 showed a tumor stromal–dominant expression of EDB+FN, with a staining pattern consistent with an ECM localization. Of note, L19 is the antibody utilized for oncology therapeutics, including the antibody-drug conjugate MICVO. Considering the staining pattern was consistent with known EDB+FN biology, wide range of detection, and established utility for EDB+FN protein targeting in the therapeutic context, L19 was selected for use in this IHC assay.

Immunohistochemistry Assay Characterization

Extradomain-B of Fibronectin Antibody Clone Specificity

To evaluate the specificity of the L19 antibody, IHC staining was performed on a set of FFPE cell pellets representing a range of *EDB+FN* RNA expression. Detection of EDB+FN using the research-use developed assay conditions reflected RNA expression, with minimal detection in the lowest expressing cell line, Hel92.1.7, increasing to the greatest expression in the highest expressing cell line, CAKI-2 (Fig. 2A). To further verify the specificity of the L19 antibody for the EDB isoform of FN, in vitro assessment of recombinant FN protein variants with and without the isoform was performed. FN contains multiple type III domains, which include 3 splice variants: extradomain-A (EDA), EDB, and a variable region (reviewed in Efthymiou 2020[38]). The L19 antibody used in the IHC assay showed strong binding by the Octet BLI assay to both native and denatured EDB-containing FN variants, hFN_7EDB89, dissociation constant (M) = 5.382E-11 and dissociation constant (M) = 6.410E-11, respectively. There was no detectable binding between the L19 antibody and an EDA-containing FN variant hFN_11EDA12 or a non–EDB-containing FN variant hFN_S607-P1265 in either native or denatured forms at the testing concentration range, whereas the positive control antibodies showed high binding affinities to both native and denatured hFN_11EDA12 and hFN_S607-P1265 (Fig. 2B). These results demonstrate the specificity of the L19 antibody for binding to the EDB domain of FN.

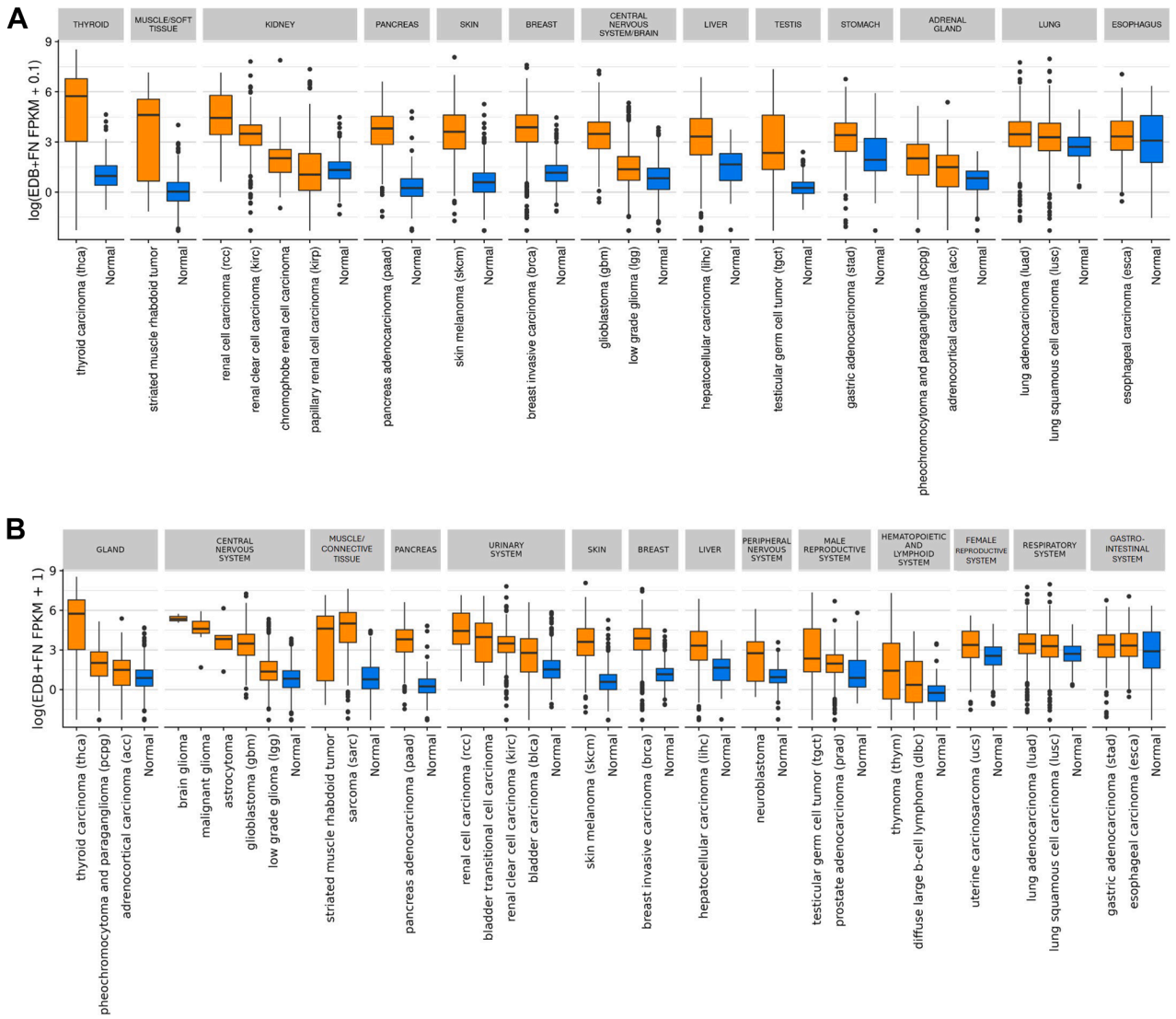

Figure 1.
Extradomain-B of fibronectin (*EDB+FN*) RNA expression analysis from publicly available data. (A) Boxplots comparing tumor and normal RNA expression of *EDB+FN*, grouped by tissue. y-axis is log (fragments per kilobase of transcript per million mapped reads [*FPKM*] + 0.1). Shown are cancer types in which median tumor expression is significantly greater than median normal expression. (B) Boxplots comparing tumor and normal RNA expression of *EDB+FN* stratified by tissue category. y-axis is log (*FPKM* + 0.1). Shown are cancer types in which median tumor expression is significantly greater than median normal expression.

Reproducibility

To evaluate the reproducibility of the research-use developed IHC assay, a two-run series of stains was performed to evaluate slides from 9 tumor samples, stained in triplicate by 2 operators. All stained samples were scored by a board-certified pathologist (T.C.). Analysis of stromal H-scores from triplicate slides stained by each operator showed high intraoperator reproducibility (%CV = 0.69 and 0.45 for operators A and B, respectively, Supplementary Fig. S2A). Comparison of stromal H-scores across triplicate slides stained by both operators showed high interoperator reproducibility (%CV = 2.49, mean bias = 3.78, LoA = −18.5 to 26.02, Supplementary Fig. S2B).

Epitope Stability

To evaluate the stability of the EDB+FN epitope in stored FFPE slides for detection by IHC, a set of prepared slides from 3 tumor tissues was stored at room temperature and stained at increasing durations of storage. All samples were scored by a board-certified pathologist (R.S.) and evaluated for consistency in stromal H-scores over time (Supplementary Fig. S3). All 3 samples showed detectable stromal EDB+FN expression over time, up to one year of storage, although some variability in EDB+FN H-scores was observed (mean %CV = 17.67). Notably, variation in scoring for each sample did not consistently trend with time, likely reflecting section-to-section heterogeneity in EDB+FN expression rather than epitope stability.

Extradomain-B of Fibronectin Protein Expression in Tumor and Normal Tissue

To verify the performance of the research-use-developed IHC assay on a larger set of tumor samples and to characterize

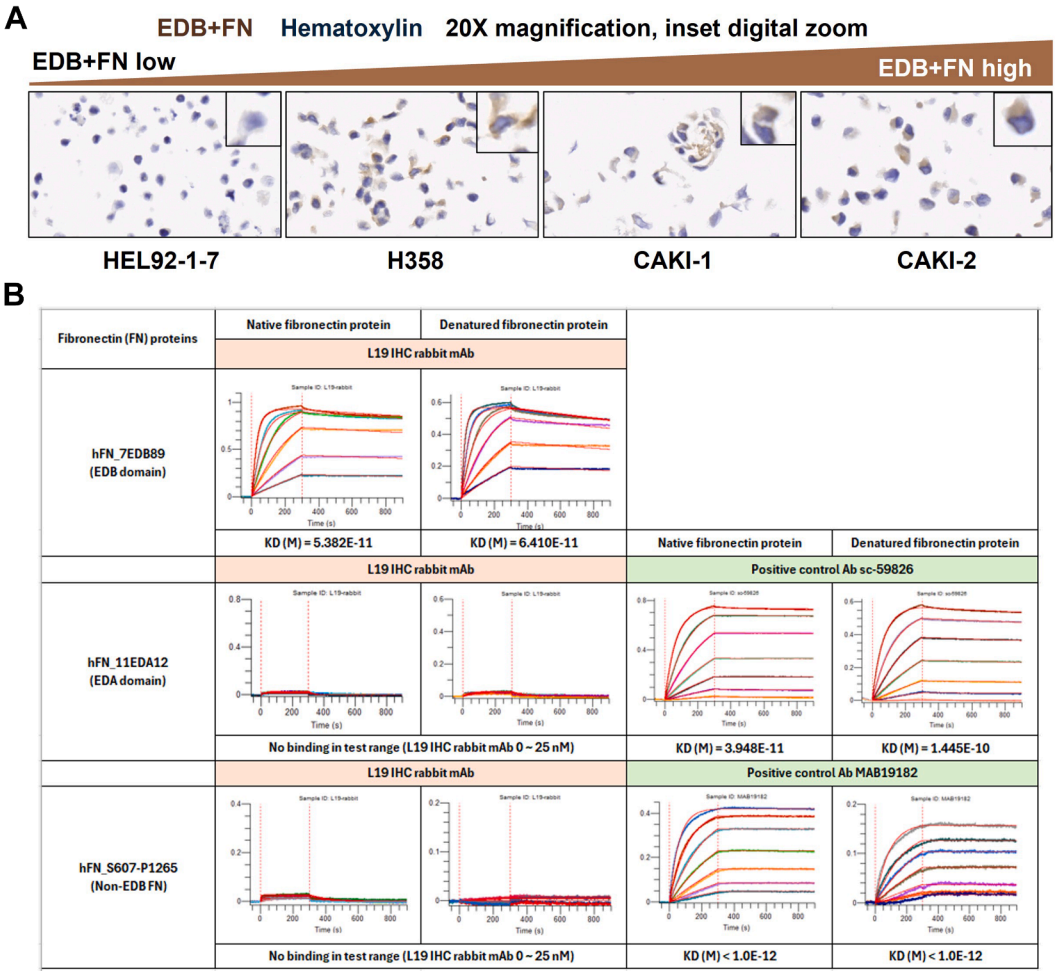

Figure 2.
Characterization of L19 immunohistochemistry (IHC) rabbit monoclonal antibody (mAb) specificity for the extradomain-B (EDB) isoform of fibronectin. (A) EDB of fibronectin IHC staining (brown) and nuclear counterstaining (blue) of formalin-fixed paraffin-embedded cell pellets using the optimized IHC assay conditions with rabbit L19 mAb. Cell lines were selected based on EDB of fibronectin RNA expression, ranging from low (HEL92-1-7) to high (CAKI-2). (B) Antibody specificity was evaluated using Octet BLI analysis. The binding affinities between L19 IHC rabbit mAb, as well as positive control antibodies, and recombinant fibronectin variants, with or without the EDB domain, in both native and heat-denatured forms were measured and represented as the dissociation constant. EDA, extradomain-A isoform of fibronectin.

EDB+FN protein expression across human solid cancer types, EDB+FN protein expression was evaluated by IHC in either whole-tissue FFPE sections or multitissue FFPE sections of tumors from 210 individuals representing 10 solid tumor cancer types. Selected cancer types included those with high *EDB+FN* expression by RNA and those of clinical interest due to high unmet medical need. EDB+FN expression was scored separately in the tumor stroma, cancer cells, and total expression (including both tumor stromal and cancer cell membrane expression). An FFPE normal tissue microarray was evaluated and scored in parallel. EDB+FN protein was broadly and differentially expressed across multiple human tumor types, including thyroid cancer, HNSCC, TNBC, and hormone receptor-positive breast cancer, hepatocellular carcinoma, soft tissue sarcoma, primarily ductal adenocarcinoma, NSCLC, and ovarian cancer, with high disease-specific expression evidenced by lack of staining in corresponding normal tissue sections (Fig. 3A). The cancer types tested by IHC showed a range of H-scores for the respective compartments evaluated (Fig. 3B). EDB+FN was expressed predominantly in tumor stroma (Supplementary Fig. S4) while cancer cell expression of EDB+FN was rare, with occasional cytoplasmic EDB+FN staining observed across most cancer types tested and infrequent cancer cell membrane expression detected in approximately half of the cancer types (Fig. 3B). Tumor stromal H-scores were proportionally higher, and total H-scores were lower because the weak or absent cancer cell membrane staining included in the total H-score diluted the stronger tumor stromal expression over a broader area. The expression pattern was disease-specific, with EDB+FN expression observed specifically in tumor-induced stroma of all tumor types, with little to no expression in normal tissues (Fig. 3C). Total expression scores showed similar trends to stromal expression scores, reflective of the most widespread and robust expression being localized in tumor stroma and minimal expression in normal tissues (Fig. 3D). Overall, thyroid cancer and HNSCC samples demonstrated the strongest and most abundant EDB+FN stromal staining of the cancer types tested, and thyroid cancer, TNBC, and HNSCC showed the highest proportion of samples with stromal H-scores $\geq$200 of the tested cancer types. Renal cell carcinoma showed the lowest expression, with a high incidence of samples with no EDB+FN staining.

The relationship between the amount of tumor stroma and extent of stromal EDB+FN expression was explored, and no

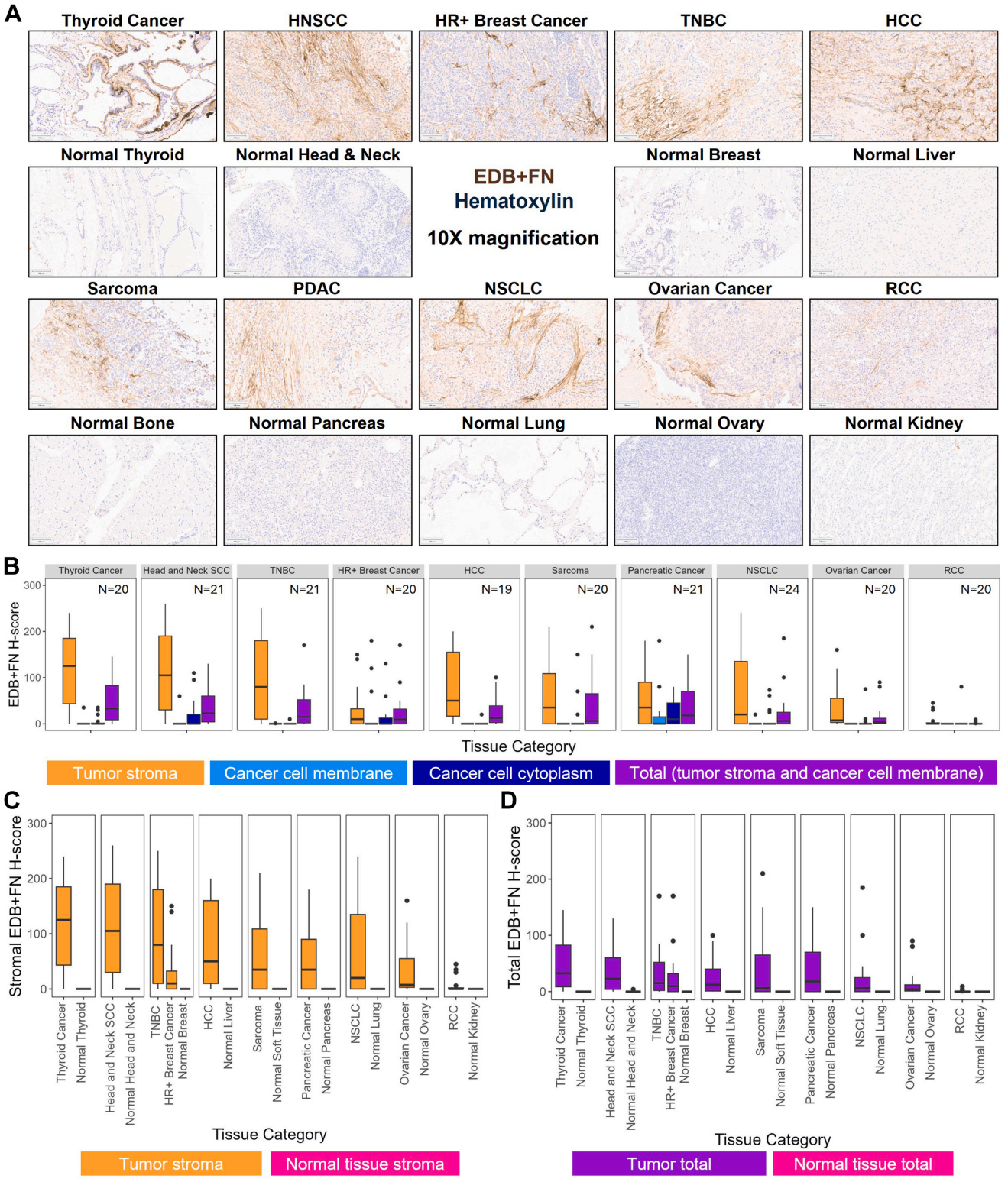

Figure 3.

Extradomain-B of fibronectin (EDB+FN) protein expression analysis in human tumor and normal tissue samples using the research-use–developed immunohistochemistry assay. (A) Representative images of EDB+FN staining (brown) and nuclei (blue) in tumor tissue compared with normal tissue. (B) H-scores of EDB+FN expression in tumor stroma (orange), cancer cell membrane (light blue), cancer cell cytoplasm (dark blue), and total, considering stroma and cancer cell membrane, collectively (purple). N = 19 to 24 samples per cancer type. (C) Stromal H-scores of EDB+FN expression in tumor (orange) compared with normal tissues (pink). (D) Total H-scores of EDB+FN expression in tumor (purple) compared with normal tissues (pink). HCC, hepatocellular carcinoma; HNSCC, head and neck squamous cell carcinoma; HR+, hormone receptor-positive; NSCLC, non–small cell lung cancer; PDAC, primarily ductal adenocarcinoma; RCC, renal cell carcinoma; TNBC, triple-negative breast cancer.

strong correlations were observed within the tumor samples of any cancer types studied (Fig. 4), highlighting that EDB+FN expression cannot be inferred based on the stromal content of a tumor, suggestive of heterogeneous EDB+FN protein expression within the TME.

Taken together, these findings show considerably more staining in tumor stroma than in cancer cells, with little to no EDB+FN protein expression observed in normal human tissue samples.

Digital Pathology

While manual pathologist scoring remains the standard for both research use and clinical IHC assays, digital pathology algorithms are beginning to emerge. To demonstrate an accessible approach to digitize scoring of a noncellular protein and to facilitate high-throughput, low-cost assessment of EDB+FN protein expression across samples from both human and preclinical models, a digital pathology assay was developed for EDB+FN (Fig. 5A). Digital H-scores determined using this algorithm correlated with pathologist H-scores, both on the sample set used for algorithm training (mean bias = 26.92, LoA = −90.66 to 144.51) (Fig. 5B) and an independent set of validation samples (mean bias = 11.25, LoA = −103.66 to 126.16) (Fig. 5C). Reproducibility of this algorithm was evaluated using the two-run pilot series of 9 tumor samples stained by 2 operators as described above for evaluating the IHC assay. Digital scoring was performed on slide scans from all slides stained in this series and evaluated for intrarun and interrun reproducibility. Intrarun reproducibility was high for both runs using the developed algorithm (%CV = 23.3 and 18.7 for run A and B, respectively, Supplementary Fig. S5A), although it showed higher variability compared with pathologist scoring. The sample sets with the highest variability tended to be poor-quality sections, including those with folds or tears, which impacted the evaluable area for the algorithm, amplifying the effects of heterogeneity of EDB+FN expression. This was especially apparent in one outlier, in which replicate samples showed substantial variation in total evaluable area due to technical artifacts. The interrun reproducibility showed some agreement, with a systemic positive bias for run A compared with run B (mean bias = 17.53, LoA = −23.07 to 58.11 for interoperator reproducibility, Supplementary Fig. S5B).

Discussion

This study described the development of a novel assay and scoring method to detect the expression of the non–cell-associated protein EDB+FN in the tumor stroma of human FFPE tumor tissue samples. The EDB+FN IHC assay revealed broad tumor-specific expression of EDB+FN across various cancer types, primarily in tumor stroma, with negligible expression in normal tissue. The highly differential expression of EDB+FN in cancer compared with normal tissue confirms EDB+FN as a promising therapeutic target. Moreover, although FN and EDB+FN are abundantly expressed in tumor stroma, this study found that percent stroma was not predictive of EDB+FN expression, indicating heterogeneous expression of EDB+FN in tumor stroma.

Although assays have been previously developed to detect EDB+FN expression for targeted EDB+FN treatments,[30,34] one of the major limitations of these assays was that they were designed for use with frozen samples, whereas preclinical and clinical samples are more often processed as FFPE.[30,37,38] Because EDB+FN is a tumor-specific ECM protein and not cell membrane-associated, no standardized and validated scoring method existed to quantify its expression or characterize its localization in tumor stroma, cancer cell membrane, and cancer cell cytoplasm. The EDB+FN IHC assay addresses and builds on these challenges. It was developed for use in FFPE samples rather than frozen tissue samples, utilized a comprehensive scoring methodology (adapted from the cell-based H-scoring methodology) to allow for characterization of heterogeneous EDB+FN expression patterns within tumors, including

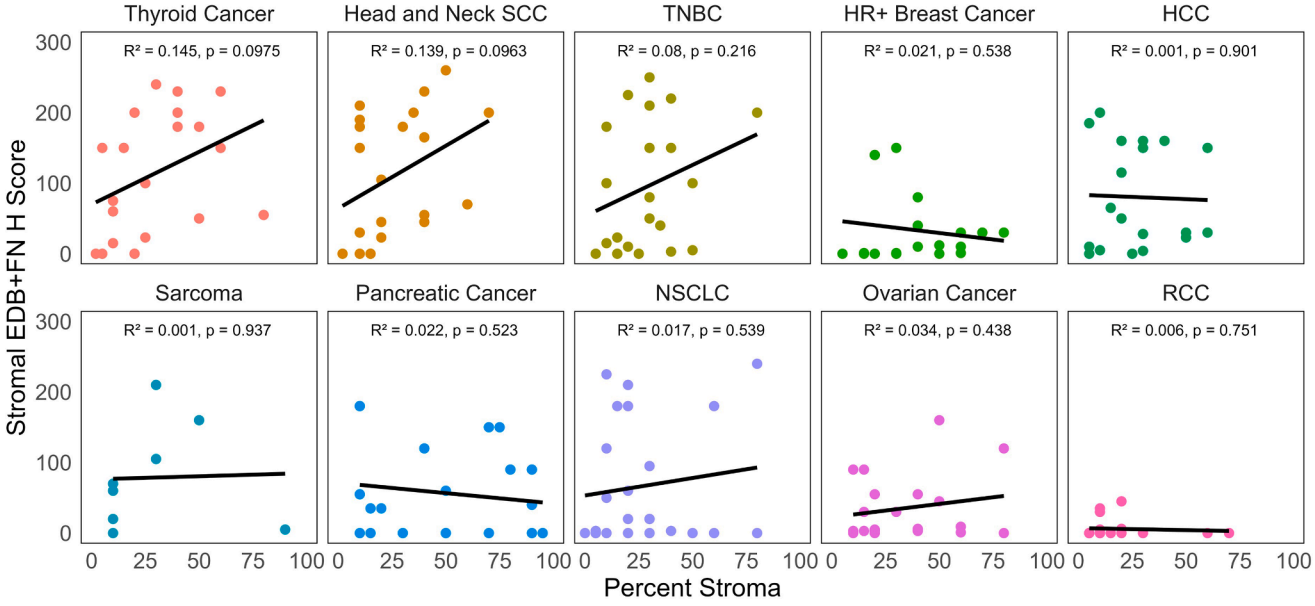

Figure 4.
Relationship between tumor stromal extradomain-B of fibronectin (EDB+FN) protein expression and percent stroma. Correlation analysis of stromal EDB+FN H-scores, determined by immunohistochemistry, and percent stroma, scored from serial hematoxylin and eosin slides. N = 19 to 24 tumor samples per tumor type. Each point represents one tumor sample. Pearson correlations are shown for each cancer type, denoted by black lines. HCC, hepatocellular carcinoma; HR+, hormone receptor-positive; NSCLC, non–small cell lung cancer; RCC, renal cell carcinoma; SCC, squamous cell carcinoma; TNBC, triple-negative breast cancer.

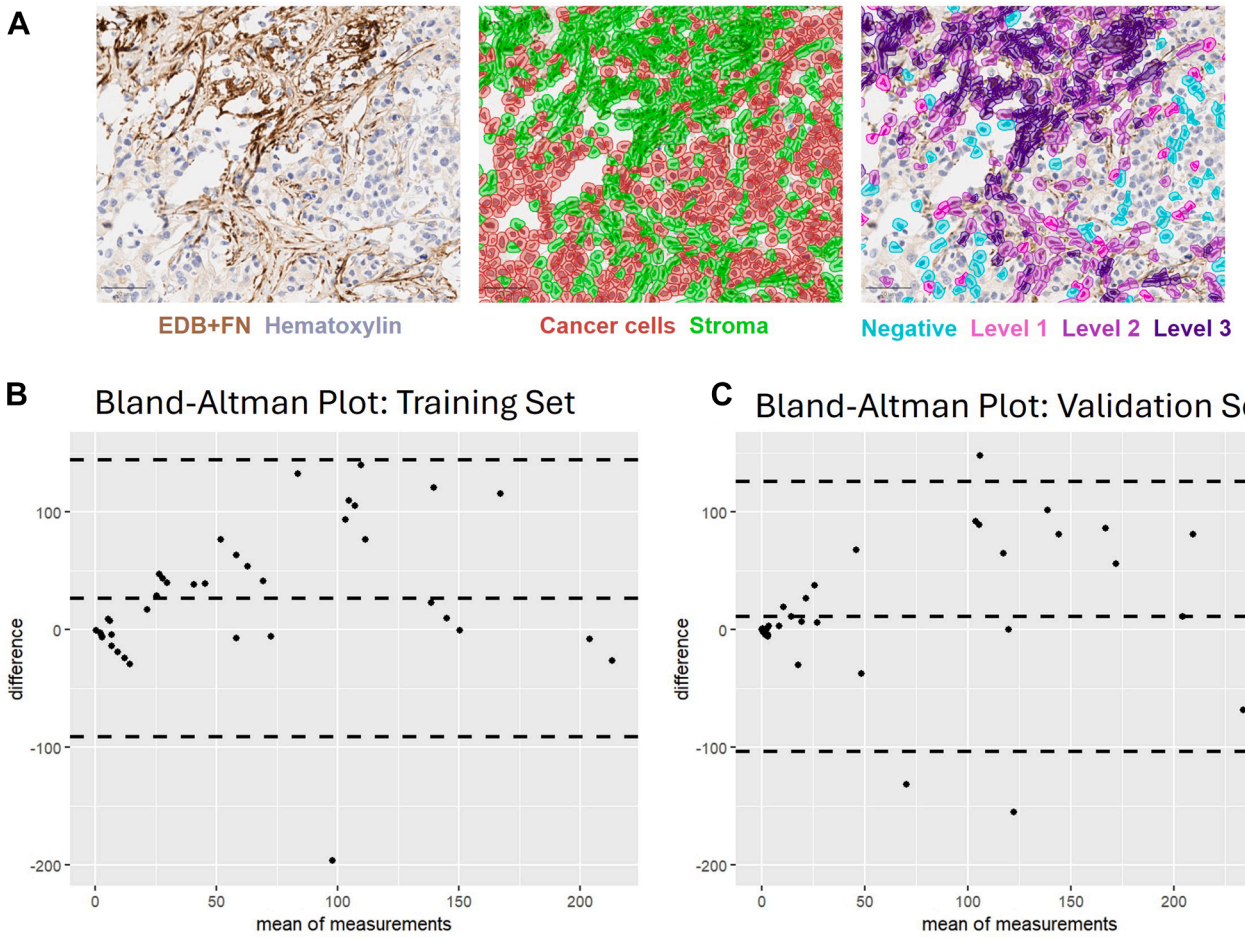

Figure 5.
Development of a digital pathology algorithm using QuPath to perform high-throughput scoring of extradomain-B of fibronectin (EDB+FN) protein expression. (A) Representative images of digital pathology model training and application for identification of tumor (red) and stroma (green), from EDB+FN immunohistochemistry-stained samples, and application of thresholding to classify stromal areas based on intensity of EDB+FN immunohistochemistry staining (blue and purple shades). The example shown is a triple-negative breast cancer sample at ×20 magnification. (B) Bland–Altman analysis of agreement of digital H-scores with pathologist-generated tumor stromal H-scores in a set of randomly selected samples (n = 40) used for digital pathology model training ("training set"). (C) Bland–Altman analysis of agreement of digital H-scores with pathologist-generated stromal H-scores for a separate set of randomly selected tumor samples (n = 40) used to validate the digital pathology model ("validation set").

both cellular and noncellular localization, and quantified inter-cancer-type and intracancer-type variation.

The developed assay shows strong proof-of-concept for staining and quantification of EDB+FN in FFPE tissue. Staining of cell pellets with variable levels of EDB+FN expression demonstrated specificity of the antibody reagent for the IHC assay, and specificity of the clone was also demonstrated by biolayer interferometry, which supports but does not replace the IHC assay–specific specificity controls. Building on these preliminary specificity findings, future studies of IHC assay–specific positive and negative controls, including development of calibration standards, could further clarify specificity of this IHC method for detection of EDB+FN in FFPE tissue samples and aid in assay transfer between laboratories. The pilot study conducted here to assess intrarun and interrun reproducibility of IHC staining found a high degree of reproducibility as assessed by manual pathologist scoring both within and between runs performed by separate technicians. Additional development, including expanded evaluation of staining reproducibility, development of calibration methodology for transfer between laboratories or staining platforms, and assessment of the consistency of the scoring algorithm across multiple pathologists, is warranted to further validate the assay. Importantly, in contrast to poor epitope stability previously reported for frozen tissue sections,[37,40] the EDB+FN epitope was detected in FFPE tissue sections using the research-use–developed IHC assay for at least 52 weeks after sectioning. While the 3 samples evaluated in the pilot testing for epitope stability did not show consistent loss of antigen detection over time, the variability that was observed in H-scores could be reflective of heterogeneous EDB+FN expression. A larger-scale stability study, including evaluation of additional samples and assessment of other preanalytical conditions, is needed to fully assess epitope stability. If, after expanded reproducibility and stability testing, the developed methods and algorithm for assessment of EDB+FN in FFPE tissues maintain high reproducibility and improved epitope stability compared with frozen sections, then this would expand the potential utility of the assay more broadly to both research and potential future development into a laboratory-developed test for use in clinical settings.

While board-certified pathologist scoring is the gold standard to evaluate IHC expression in clinical samples, the field is rapidly moving toward digital pathology, which is routinely used in the preclinical setting and utilization is increasing in the clinical setting, as demonstrated by the development of quantitative

continuous scoring for Trop2 expression.[51] Here, a novel artificial intelligence–powered digital pathology algorithm was developed for an extracellular protein with a custom algorithm for the generation of digital stromal H-scores in a scalable, high-throughput manner. Although the developed algorithm showed high intrarun reproducibility, the variability was substantially higher than that observed in pathologist scoring. This could be due to a combination of variability in evaluable area due to technical artifacts, such as tissue folding or scanning artifacts, and heterogeneity of EDB+FN protein expression, which manifests most strongly in samples with intermediate scores rather than samples with more uniform weak or robust EDB+FN expression. This was observed most notably in one outlier sample set in which there were substantial folding artifacts and heterogeneous intermediate EDB+FN expression. Furthermore, pilot analysis of intrarun reproducibility of staining showed a systemic positive bias for run A over run B, potentially reflecting a slight increase in staining intensity in run A, which impacted the algorithm scoring but not pathologist scoring. Inclusion of run controls could be explored to improve calibration of digital scoring between runs.

Acknowledging that the digital algorithm, in its current research-use form, does not match or outperform pathologist scoring, the developed algorithm has advantages in allowing for rapid and cost-effective screening of samples for indication and in vivo model selection and for mechanism of action studies, accelerating research for EDB+FN-targeting therapeutics. This digitization of EDB+FN protein expression also serves as a foundation for the development of future continuous and spatial proximity scoring approaches to expand on the capabilities of pathologist scoring and aid in identifying scoring metrics that most effectively capture the biology of EDB+FN expression. Notably, the developed algorithm utilizes existing open-source digital pathology tools within Qupath, highlighting the accessibility of digital pathology, even for a noncell surface target.

Considering the interest in EDB+FN as a clinical target, as well as the complete sequence conservation of EDB+FN across humans, nonhuman primates, and rodents, the EDB+FN IHC assay using traditional and/or digital scoring will be advantageous for future work that aims to evaluate protein expression in tumor samples regardless of species. This work will aid research studies investigating whether the intensity, distribution, and/or localization of EDB+FN protein expression correlates with response to EDB+FN-targeting therapies such as MICVO and could be further developed into a laboratory-developed test for use in clinical settings.

This study demonstrates the development and deployment of a specific and reproducible research-use IHC assay for detection of EDB+FN in FFPE tumor tissue samples. EDB+FN showed tumor stroma-specific expression and broad distribution of expression across cancer types, but notably did not correlate with percent stroma, suggesting heterogeneous expression within cancer stroma. The developed scoring approach, which adapts traditional H-score methodology for separate area-based cancer cell and stromal scoring, establishes a proof-of-concept for quantification of intensity and distribution of a primarily extracellular target. The accompanying digital pathology algorithm allows for rapid and convenient testing of samples and can serve as a basis for development of continuous or spatial proximity scoring. As such, the use of both traditional and digital pathology to evaluate the intensity and distribution of EDB+FN expression and potential correlations with tissue architecture and cancer pathology will be the focus of future studies.

Acknowledgments

This study was conceived and designed by Pyxis Oncology, who also performed initial assay development and complete development of the digital scoring algorithm. Further assay development, characterization, and pathologist scoring were performed by Discovery Life Sciences under the direction of Pyxis Oncology. JetPub Scientific Communications LLC assisted the authors in the initial formatting of this manuscript.

Author Contributions

S.L.L. performed conceptualization, investigation, validation, methodology, formal analysis, writing, review, and editing. C.S. performed conceptualization, investigation, validation, methodology, formal analysis, writing, review, and editing. L.D. performed conceptualization, investigation, validation, methodology, formal analysis, review, and editing. A.M.Q. performed conceptualization, investigation, validation, methodology, review, and editing. T.B. performed investigation, validation, methodology, and review and editing. T.C. performed investigation, validation, methodology, and review and editing. T.D. performed investigation, validation, methodology, and review and editing. R.S. performed investigation, validation, methodology, and review and editing. M.L.C. performed writing, review, and editing. J.P. performed review and editing.

Data Availability

The data that support the findings of this study are available upon reasonable request from the corresponding author, Sara L. Lewandowski.

Funding

This work was supported by Pyxis Oncology Inc.

Declaration of Competing Interest

S.L. Lewandowski, C. Shen, and M.L. Crochiere are current employees of Pyxis Oncology. A.M. Quigley, L. Diao, and J. Pinkas are former employees of Pyxis Oncology. T. Dolker and R. Siderits are current employees of Discovery Life Sciences. T. Brennan is a former employee of Discovery Life Sciences.

Ethics Approval and Consent to Participate

All human samples were deidentified and obtained from commercial sources operating under their respective institutional review board-approved protocols.

Supplementary Material

The online version contains supplementary material available at https://doi.org/10.1016/j.labinv.2026.106156.

References

1. Miller KD, Nogueira L, Devasia T, et al. Cancer treatment and survivorship statistics, 2022. *CA Cancer J Clin*. 2022;72(5):409–436. https://doi.org/10.3322/caac.21731
2. Zhao Y, Bai Y, Shen M, Li Y. Therapeutic strategies for gastric cancer targeting immune cells: future directions. *Front Immunol*. 2022;13:992762. https://doi.org/10.3389/fimmu.2022.992762

3. Xue R, Zhang Q, Cao Q, et al. Liver tumour immune microenvironment subtypes and neutrophil heterogeneity. *Nature*. 2022;612(7938):141–147. https://doi.org/10.1038/s41586-022-05400-x
4. Pitt JM, Marabelle A, Eggermont A, Soria J-C, Kroemer G, Zitvogel L. Targeting the tumor microenvironment: removing obstruction to anticancer immune responses and immunotherapy. *Ann Oncol*. 2016;27(8):1482–1492. https://doi.org/10.1093/annonc/mdw168
5. Klemm F, Joyce JA. Microenvironmental regulation of therapeutic response in cancer. *Trends Cell Biol*. 2015;25(4):198–213. https://doi.org/10.1016/j.tcb.2014.11.006
6. Gajewski TF. Failure at the effector phase: immune barriers at the level of the melanoma tumor microenvironment. *Clin Cancer Res*. 2007;13(18):5256–5261. https://doi.org/10.1158/1078-0432.CCR-07-0892
7. Baskar R, Lee KA, Yeo R, Yeoh K-W. Cancer and radiation therapy: current advances and future directions. *Int J Med Sci*. 2012;9(3):193–199. https://doi.org/10.7150/ijms.3635
8. Weber JS, O'Day S, Urba W, et al. Phase I/II study of ipilimumab for patients with metastatic melanoma. *J Clin Oncol*. 2008;26(36):5950–5956. https://doi.org/10.1200/JCO.2008.16.1927
9. Phan GQ, Yang JC, Sherry RM, et al. Cancer regression and autoimmunity induced by cytotoxic T lymphocyte-associated antigen 4 blockade in patients with metastatic melanoma. *Proc Natl Acad Sci USA*. 2003;100(14):8372–8377. https://doi.org/10.1073/pnas.1533209100
10. Zhao C, Zeng Y, Kang N, Liu Y. A new perspective on antiangiogenic antibody drug resistance: biomarkers, mechanisms, and strategies in malignancies. *Drug Dev Res*. 2024;85(6):e22257. https://doi.org/10.1002/ddr.22257
11. Baghban R, Roshangar L, Jahanban-Esfahlan R, et al. Tumor microenvironment complexity and therapeutic implications at a glance. *Cell Commun Signal*. 2020;18(1):59. https://doi.org/10.1186/s12964-020-0530-4
12. Huelsken J, Hanahan D. A subset of cancer-associated fibroblasts determines therapy resistance. *Cell*. 2018;172(4):643–644. https://doi.org/10.1016/j.cell.2018.01.028
13. Jurj A, Ionescu C, Berindan-Neagoe I, Braicu C. The extracellular matrix alteration, implication in modulation of drug resistance mechanism: friends or foes? *J Exp Clin Cancer Res*. 2022;41(1):276. https://doi.org/10.1186/s13046-022-02484-1
14. Kramer CJH, Vangangelt KMH, van Pelt GW, Dekker TJA, Tollenaar RAEM, Mesker WE. The prognostic value of tumour–stroma ratio in primary breast cancer with special attention to triple-negative tumours: a review. *Breast Cancer Res Treat*. 2019;173(1):55–64. https://doi.org/10.1007/s10549-018-4987-4
15. Zhao Y, Shen M, Wu L, et al. Stromal cells in the tumor microenvironment: accomplices of tumor progression? *Cell Death Dis*. 2023;14(9):587. https://doi.org/10.1038/s41419-023-06110-6
16. Brassart-Pasco S, Brézillon S, Brassart B, Ramont L, Oudart J-B, Monboisse JC. Tumor microenvironment: extracellular matrix alterations influence tumor progression. *Front Oncol*. 2020;10:397. https://doi.org/10.3389/fonc.2020.00397
17. Bonnans C, Chou J, Werb Z. Remodelling the extracellular matrix in development and disease. *Nat Rev Mol Cell Biol*. 2014;15(12):786–801. https://doi.org/10.1038/nrm3904
18. da Silva PHR, Borges BC, Uehara IA, Soldi LR, de Araújo RA, Silva MJB. Chemokines and the extracellular matrix: set of targets for tumor development and treatment. *Cytokine*. 2021;144:155548. https://doi.org/10.1016/j.cyto.2021.155548
19. Micke P, Strell C, Mattsson J, et al. The prognostic impact of the tumour stroma fraction: a machine learning-based analysis in 16 human solid tumour types. *EBioMedicine*. 2021;65:103269. https://doi.org/10.1016/j.ebiom.2021.103269
20. Arnold SA, Loomans HA, Ketova T, Andl CD, Clark PE, Zijlstra A. Urinary oncofetal ED-A fibronectin correlates with poor prognosis in patients with bladder cancer. *Clin Exp Metastasis*. 2016;33(1):29–44. https://doi.org/10.1007/s10585-015-9754-x
21. Vaidya A, Wang H, Qian V, Gilmore H, Lu Z-R. Overexpression of extradomain-B fibronectin is associated with invasion of breast cancer cells. *Cells*. 2020;9(8):1826. https://doi.org/10.3390/cells9081826
22. Hall RC, Vaidya AM, Schiemann WP, Pan Q, Lu Z-R. RNA-Seq analysis of extradomain A and extradomain B fibronectin as extracellular matrix markers for cancer. *Cells*. 2023;12(5):685. https://doi.org/10.3390/cells12050685
23. Matsumoto E, Yoshida T, Kawarada Y, Sakakura T. Expression of fibronectin isoforms in human breast tissue: production of extra domain A+/extra domain B+ by cancer cells and extra domain A+ by stromal cells. *Jpn J Cancer Res*. 1999;90(3):320–325. https://doi.org/10.1111/j.1349-7006.1999.tb00750.x
24. Petrini I, Barachini S, Carnicelli V, et al. ED-B fibronectin expression is a marker of epithelial-mesenchymal transition in translational oncology. *Oncotarget*. 2017;8(3):4914–4921. https://doi.org/10.18632/oncotarget.13615
25. Berndt A, Borsi L, Luo X, Zardi L, Katenkamp D, Kosmehl H. Evidence of ED-B+ fibronectin synthesis in human tissues by non-radioactive RNA in situ hybridization. Investigations on carcinoma (oral squamous cell and breast carcinoma), chronic inflammation (rheumatoid synovitis) and fibromatosis (Morbus Dupuytren). *Histochem Cell Biol*. 1998;109(3):249–255. https://doi.org/10.1007/S004180050224
26. Menrad A, Menssen HD. ED-B fibronectin as a target for antibody-based cancer treatments. *Expert Opin Ther Targets*. 2005;9(3):491–500. https://doi.org/10.1517/14728222.9.3.491
27. Saw PE, Xu X, Kang BR, et al. Extra-domain B of fibronectin as an alternative target for drug delivery and a cancer diagnostic and prognostic biomarker for malignant glioma. *Theranostics*. 2021;11(2):941–957. https://doi.org/10.7150/thno.44948
28. Saw PE, Kim S, Lee I, et al. Aptide-conjugated liposome targeting tumor-associated fibronectin for glioma therapy. *J Mater Chem B*. 2013;1(37):4723–4726. https://doi.org/10.1039/c3tb20815j
29. Han Z, Lu Z-R. Targeting fibronectin for cancer imaging and therapy. *J Mater Chem B*. 2017;5(4):639–654. https://doi.org/10.1039/c6tb02008a
30. Hooper AT, Marquette K, Chang C-PB, et al. Anti-extra domain B splice variant of fibronectin antibody–drug conjugate eliminates tumors with enhanced efficacy when combined with checkpoint blockade. *Mol Cancer Ther*. 2022;21(9):1462–1472. https://doi.org/10.1158/1535-7163.MCT-22-0099
31. Li F, Hooper AT, Golas J, Chang C-PB, Neubert H, King L. Evaluation of EDB fibronectin in plasma, patient-derived xenograft formalin-fixed paraffin-embedded and fresh frozen tumor tissues using immunoaffinity LC-MS/MS. *J Proteome Res*. 2022;21(10):2331–2340. https://doi.org/10.1021/acs.jproteome.2c00182
32. Poli GL, Bianchi C, Virotta G, et al. Radretumab radioimmunotherapy in patients with brain metastasis: a 124I-L19SIP dosimetric PET study. *Cancer Immunol Res*. 2013;1(2):134–143. https://doi.org/10.1158/2326-6066.CIR-13-0007
33. Erba PA, Sollini M, Orciuolo E, et al. Radioimmunotherapy with radretumab in patients with relapsed hematologic malignancies. *J Nucl Med*. 2012;53(6):922–927. https://doi.org/10.2967/jnumed.111.101006
34. Sauer S, Erba PA, Petrini M, et al. Expression of the oncofetal ED-B–containing fibronectin isoform in hematologic tumors enables ED-B–targeted 131I-L19SIP radioimmunotherapy in Hodgkin lymphoma patients. *Blood*. 2009;113(10):2265–2274. https://doi.org/10.1182/blood-2008-06-160416
35. Pini A, Viti F, Santucci A, et al. Design and use of a phage display library. *J Biol Chem*. 1998;273(34):21769–21776. https://doi.org/10.1074/jbc.273.34.21769
36. Lieverse RIY, Marcus D, van der Wiel AMA, et al. Human fibronectin extra domain B as a biomarker for targeted therapy in cancer. *Mol Oncol*. 2020;14(7):1555–1568. https://doi.org/10.1002/1878-0261.12705
37. Schliemann C, Palumbo A, Zuberbühler K, et al. Complete eradication of human B-cell lymphoma xenografts using rituximab in combination with the immunocytokine L19-IL2. *Blood*. 2009;113(10):2275–2283. https://doi.org/10.1182/blood-2008-05-160747
38. Puca E, Probst P, Stringhini M, et al. The antibody-based delivery of interleukin-12 to solid tumors boosts NK and CD8+ T cell activity and synergizes with immune checkpoint inhibitors. *Int J Cancer*. 2020;146(9):2518–2530. https://doi.org/10.1002/ijc.32603
39. Schwager K, Villa A, Rösli C, Neri D, Rösli-Khabas M, Moser G. A comparative immunofluorescence analysis of three clinical-stage antibodies in head and neck cancer. *Head Neck Oncol*. 2011;3(1):25. https://doi.org/10.1186/1758-3284-3-25
40. Kaczmarek J, Castellani P, Nicolo G, Spina B, Allemanni G, Zardi L. Distribution of oncofetal fibronectin isoforms in normal, hyperplastic and neoplastic human breast tissues. *Int J Cancer*. 1994;59(1):11–16. https://doi.org/10.1002/ijc.2910590104
41. McCarty KS Jr, Miller LS, Cox EB, Konrath J, McCarty KS Sr. Estrogen receptor analyses. Correlation of biochemical and immunohistochemical methods using monoclonal antireceptor antibodies. *Arch Pathol Lab Med*. 1985;109(8):716–721.
42. Wen Z, Luo D, Wang S, et al. Deep learning–based H-score quantification of immunohistochemistry-stained images. *Mod Pathol*. 2024;37(2):100398. https://doi.org/10.1016/j.modpat.2023.100398
43. Zhou Y, Tao L, Qiu J, et al. Tumor biomarkers for diagnosis, prognosis and targeted therapy. *Signal Transduct Target Ther*. 2024;9(1):132. https://doi.org/10.1038/s41392-024-01823-2
44. Robinson JT, Thorvaldsdóttir H, Winckler W, et al. Integrative genomics viewer. *Nat Biotechnol*. 2011;29(1):24–26.
45. Kent WJ. BLAT—the BLAST-like alignment tool. *Gen Res*. 2002;12(4):656–664.
46. Wickham H. *ggplot2: Elegant Graphics for Data Analysis. New York: Springer-Verlag;* 2016. ISBN 978-3-319-24277-4.
47. Wickham H, François R, Henry L, Müller K, Vaughan D. *dplyr: A Grammar of Data Manipulation*. 2026. R package version 1.2.1.
48. Wickham H, Vaughan D, Girlich M. *tidyr: Tidy Messy Data*. 2026. R package version 1.3.2.
49. Lehnert B. *BlandAltmanLeh: Plots (Slightly Extended) Bland-Altman Plots*. 2015. R package version 0.3.1.
50. Bankhead P, Loughrey MB, Fernández JA, et al. QuPath: Open source software for digital pathology image analysis. *Sci Rep*. 2017;7(1):16878.
51. Garassino MC, Sands J, Paz-Ares L, et al. PL02.11 normalized membrane ratio of TROP2 by quantitative continuous scoring is predictive of clinical outcomes in TROPION-Lung 01. *J Thorac Oncol*. 2024;19(10):S2–S3. https://doi.org/10.1016/j.jtho.2024.09.015